Recombination channels in CIGS thin films: impact of the Ga-profile

J. P. Teixeira,[†,‡] R. B. L. Vieira,[†] B. P. Falcão,[†] M. Edoff,[¶] P. M. P. Salomé,[‡,§] and J. P. Leitão[*,†]

†i3N and Departamento de Física, Universidade de Aveiro, Campus Universitário de Santiago, 3810-193 Aveiro, Portugal

‡INL - International Iberian Nanotechnology Laboratory, 4715-330 Braga, Portugal

¶Ångström Solar Center, Solid State Electronics, Uppsala University, Ångström Laboratory PO Box 534, SE-751 21 Uppsala, Sweden

§Departamento de Física, Universidade de Aveiro, 3810-193 Aveiro, Portugal

E-mail: joaquim.leitao@ua.pt

https://doi.org/10.1021/acs.jpcc.0c02622

Abstract

Depth bandgap profiles via a [Ga]/([Ga]+[In]) variation in the Cu(In,Ga)Se_2 (CIGS) absorber layer have been implemented as a strategy to enhance the performance of CIGS solar cells. Since the [Ga]/([Ga]+[In]) determines to a large extent the position of the conduction band minimum, different Ga-profiles lead to different electronic energy levels structures throughout the CIGS layer. In this paper, from the investigation of the dependence of the photoluminescence (PL) on excitation power and temperature, we critically analyse the impact of a notch or a linear Ga-profiles on the CIGS electronic energy levels structure and subsequent dominant recombination channels. Notwithstanding two radiative transitions involving fluctuating potentials were observed for each sample, significant differences in the luminescence resultant from the two Ga-profiles were identified. For the CIGS absorber with a notch Ga-profile, two tail-impurity radiative transitions involving equivalent donors cluster and the same deep acceptor level were ascribed to the near CIGS/CdS interface and the notch regions. The probability of radiative recombination in the two regions is discussed. For the CIGS absorber with a linear Ga-profile, two band-impurity radiative transitions involving an acceptor, with an ionization energy compatible with the V_{Cu} defect were ascribed to the region near the CIGS/CdS interface. Our results shows that the dominant acceptor defects are dependent on the Ga-profile and they also highlight the complexity of the radiative and non-radiative recombination channels revealed by a tight control of the parameters in the experiment.

Introduction

Cu(In,Ga)Se_2 (CIGS) based solar cells are the most efficient thin film technology having recently achieved a light to power conversion efficiency value of 23.35%.[1] The improvements in the performance reported in recent years have not been always followed by an increase of the open-circuit voltage (V_{OC}).[2,3] However, in the former record (22.9%),[4] the authors linked the obtained value to an effective reduction in the density of defects in the CIGS absorber

layer, which led to lower V_{OC} losses.[5,6] The improvement of the absorber quality was obtained via a modified in-depth variation of the bandgap (E_g) regarding the conventional one. This result reinforces that the implementation of an in-depth bandgap profile strategy is decisive to enhance the efficiency in CIGS based solar cells.[7–13]

The bandgap profiles in the CIGS layer have been mostly obtained by an in-depth [Ga]/([Ga]+[In]) (GGI) variation, creating a Ga-profile that is known to influence the conduction band minimum of CIGS.[14,15] Two different Ga-profiles are often implemented: i) notch profile (double-grade), a high concentration of Ga at the back surface, that decreases until a minimum value, followed by a small increase of the Ga concentration at the front surface;[9,11,16] ii) linear profile, a linear gradient with a high concentration of Ga at the back and a low concentration at the superficial region of the CIGS.[11,17,18] Both Ga-profiles will induce a back quasi-electric field that will superimpose on the random motion of the photogenerated carriers in the quasi-neutral region. Therefore, electrons will be drifted to the *pn*-heterojunction, pushing them away from the highly recombinative back interface. Hence, Ga-profiles will have an important impact in the charge carriers dynamics that at great extent dictates the performance of the solar cells. Additionally, there are several simulation studies[9,19–24] that showed the importance of the shape of the bandgap profile on the performance of the solar cells, the value of the GGI minimum, and the position of GGI minimum inside or outside the space charge region. On the other hand, a few experimental studies investigating the impact of the Ga-profile on the charge carriers dynamics, are available.[10,25–30] However, a deep understanding of the impact of the Ga-profiles on the recombination channels is still lacking. As CIGS technology approaches the ideal Shockley-Queisser limit, further improvements will strongly depend on the understanding of fundamental physical properties, such as CIGS complex electronic energy levels structure. In this way, photoluminescence (PL) may provide significant contribution.[6,18,28,30–32]

The luminescence of CIGS samples with a notch Ga-profile commonly presents two clear radiative transitions,[11,28,30,32–36] whose origin is commonly related with the characteristic

shape of the notch profile. In the case of a linear Ga-profile a broad luminescence is observed.[11,18] Different Ga-profiles will led to different electronic energy levels structures, and, more importantly, to in-depth differences in the electronic energy levels structure that meet the changes on the Ga content throughout the CIGS layer. Thus, the comparison of the luminescence between the two Ga-profiles may help on the analysis of the differences in the performance of the solar cells based on the two Ga-profiles and, ultimately, contribute to discussion of the charge carrier dynamics in both profiles. An accurate analysis of the luminescence should take into account the previous physical discussion as well as the fact that the observed radiative recombination is limited by the minority charge carriers diffusion length.

In this work, we studied by steady-state PL two CIGS samples prepared with different Ga-profiles, a three-stage sample with a typical notch Ga-profile and an in-line sample with a linear Ga-profile, and focused the discussion on the analysis of the dominant radiative and non-radiative recombination channels observed in each Ga-profile. The samples were grown at the same laboratory in the same work session, in order to minimize possible unintended differences in the physical properties of the two samples. Commonly, the works in the literature, deal with samples with only one type of Ga-profile, which means the comparison between different profiles involves samples grown by different groups with necessarily more degrees of freedom than the presented in this work. The impact of different Ga-profiles in the nature of the dominant radiative and non-radiative recombination channels was deeply analysed, highlighting the importance of understanding the recombination channels in CIGS.

Methods

Two samples were grown at the Ångström Laboratory in the same work session through: a three-stage process, which creates a notch Ga-profile (N sample) and an in-line process which creates a linear Ga-profile (L sample). The growth parameters and Ga-profiles have

been reported elsewhere,[11] being the latter presented below (see insets in Fig. 4). The measured power conversion efficiency of both solar cells, with no anti-reflective coatings or post-deposition alkali treatment, are 17.0% and 16.3% for the N and L samples, respectively.

PL measurements on SLG/Mo/CIGS/CdS based samples were carried out using a Bruker IFS 66v Fourier Transform Infrared (FTIR) spectrometer equipped with a Ge diode detector. The correction of the detectivity of the detector was performed in all PL spectra of the two samples. The samples were inserted in a helium gas flow cryostat, which allowed to change the temperature in the range 4-300 K. The excitation source was a 514.5 nm line of an Ar^+ ion laser, and the laser power was measured at the front of the cryostat window. The diameter of the laser spot was approximately 1 mm.

Results

The PL spectra for the N and L samples, measured at approximately 5 K under an excitation power of 1 mW, are shown in Fig. 1(a). The signal-to-noise ratio for the PL spectrum of L sample is higher than for N sample. A radiative transition at approximately 1.015 eV dominates the two spectra (hereafter denoted by N_1 and L_1). In the case of N sample, an additional transition (N_2) at approximately 1.09 eV is observed. For both samples, the deconvolution of the radiative transitions was done by fitting the measured PL spectra with three Gaussian components. This procedure allow us to separate the individual contributions of the two transitions in the case of N sample and to identify another transition (L_2), at approximately 1.03 eV, for L sample [see Fig. 1(b) and (c)]. It is important to note that, for both samples the radiative transition N_1 and L_1 have an asymmetric shape, and for that reason both radiative transitions are described by two Gaussian components ($1'$ and 1). In order to study the dependence of the peak energy of the radiative transitions on the excitation power and temperature, we took the peak energy of Gaussian 1 from transition N_1 and L_1, since the maximum of intensity of the transition is coincident with the peak of Gaussian 1

and components 1′ mainly describe the asymmetric shape of the transition. The integrated intensity of each transition was obtained through the sum of the areas of the two components that describe the transition. The peak energies of the above transitions, extracted from the PL spectra measured at ∼5 K under an excitation power of 1 mW (Fig. 1(a)), are listed in Table 1.

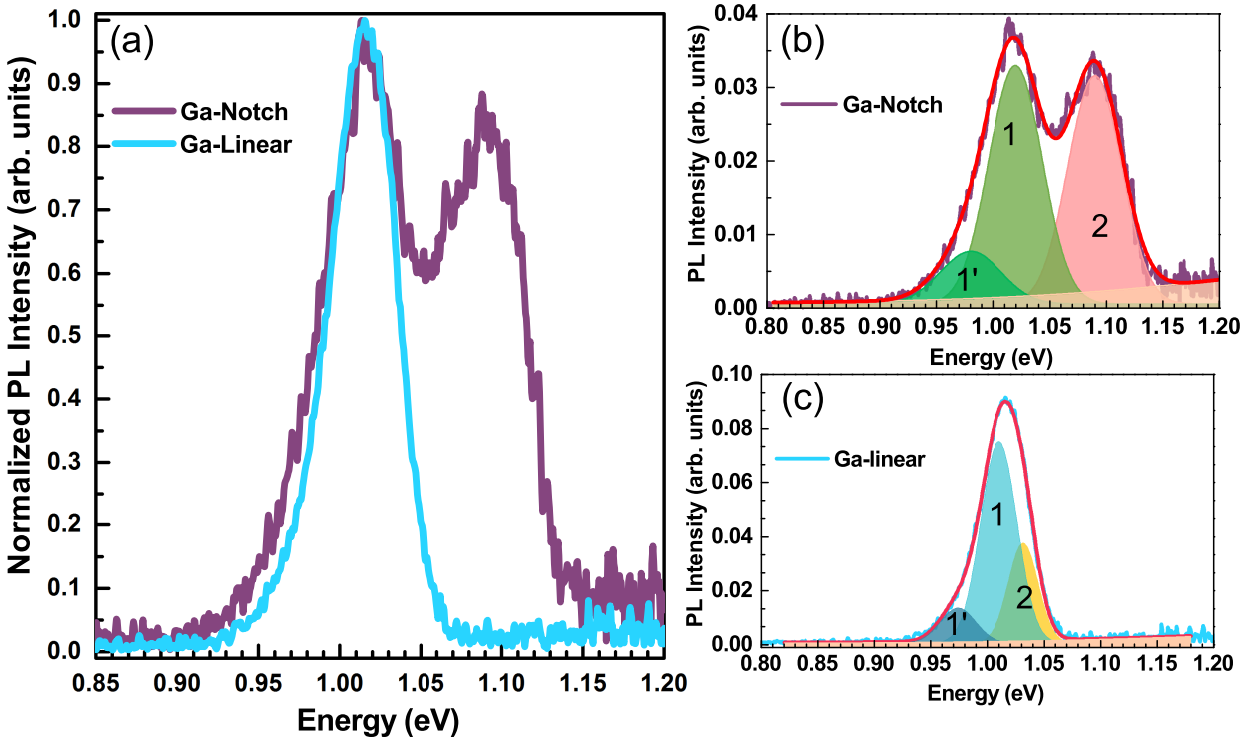

Figure 1: (a) PL spectra of N and L samples measured at ∼5 K under an excitation power of 1 mW. (b) and (c) illustrates the fitting model with Gaussian components to the PL spectra shown in (a).

Table 1: Values of the peak energy (E_p) measured at ∼5 K under 1 mW, β, and m parameter estimated for the two radiative transitions observed in N and L samples.

Sample	Transition	E_p (eV)	β (meV)	m
N	N_1	1.018	6.4 ± 0.2	1.08 ± 0.02
	N_2	1.090	5.6 ± 0.2	0.93 ± 0.04
L	L_1	1.010	2.9 ± 0.3	0.87 ± 0.01
	L_2	1.031	4.3 ± 0.2	1.21 ± 0.02

In Fig. 2 we show for both samples the dependencies of the peak energy (E_p) and PL

integrated intensity (I) of the two radiative transitions on the excitation power (P), measured at 5 K. A blueshift is observed, being parameterized by the equation:[37–40]

$$E_p = \beta \ln \left(P/P_\circ \right), \tag{1}$$

where β is a coefficient that parameterizes the energy shift, and $P_\circ$ is a fitting parameter. The estimated values of β, presented in Table 1, are in the range 2.9–6.4 meV, which are high enough to be compatible with the presence of fluctuating potentials.[37–39,41–43] In the case of N_2 transition, the blueshift is observed mainly in the lower excitation power regime. Since the shape of the low energy side of the luminescence of both samples (not shown) is not significantly affected by the excitation power, we ascribe the observed blueshift to a state filling effect.[42,44] Regarding the PL integrated intensity, the experimental data for N sample are shown in Fig. 2(c). The two transitions show a different behaviour as the excitation power is incremented: the intensity of the N_1 transition increases linearly, whereas a saturation for $P > 10$ mW is observed for the N_2 transition. In the case of L sample [Fig. 2(d)], the intensity of both transitions increases linearly with the excitation power without saturation. As shown in Fig. 2(c) and (d), the experimental data were fitted with the power law[45]

$$I \propto P^m, \tag{2}$$

where m is an adjustable parameter. The estimated values of m are in the range 0.9–1.2 and are presented in Table 1. Values around 1 are consistent with transitions involving fluctuating potentials.[18,38,39,41–43,46–48]

Figure 3 shows the dependence of the luminescence of N and L samples on temperature, studied under an excitation power of 3.5 and 19.1 mW, respectively. Due to the low relative intensity of transition L_2 at low excitation powers (see Fig. 1), a higher excitation power was used for L sample, in comparison with the one of N sample, to allow a deeper investigation of all transitions. As shown in Fig. 3(c), with the increase of the temperature, the PL integrated

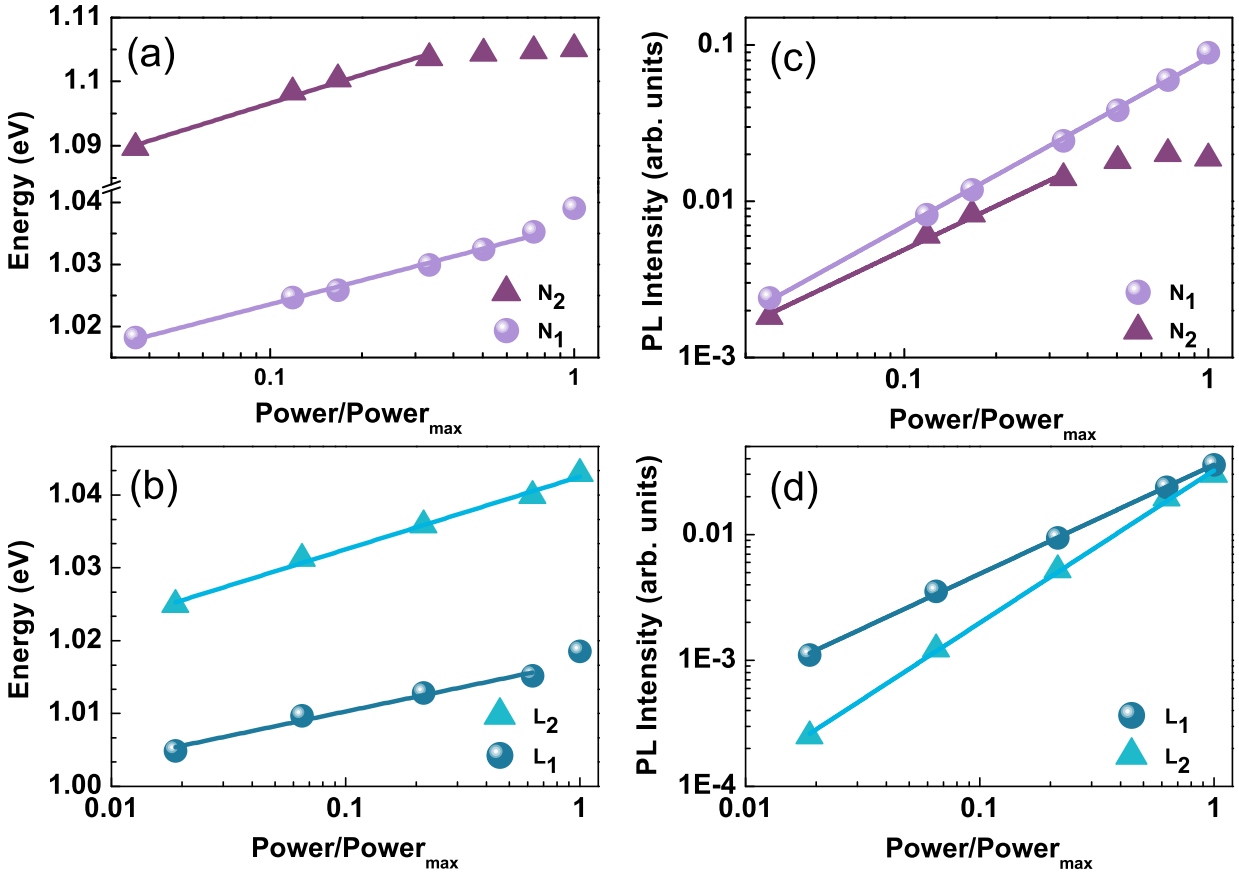

Figure 2: Dependence of the peak energy [(a), (b)] and PL integrated intensity [(c), (d)] of the two radiative transitions for N (top row) and L (bottom row) samples, on the excitation power, the data of both samples is normalized to the excitation power maximum value of 30 mW. The measurements were performed at 5 K. The solid lines in (a) and (c) represented the fit of Eq. 1 and in (c) and (d) represented the fit of Eq. 2 to the experimental data.

intensity of both radiative transitions for L sample evidence a common behaviour:[18,49] a small decrease for low temperatures (5–40 K), followed by a stronger reduction until the thermal quenching at approximately 240 K. Regarding N sample, the behaviours of the two transitions are quite different:[33] as the temperature is incremented, N_2 transition suffers a thermal quenching at approximately 40 K, whereas in the same temperature regime, the relative PL integrated intensity of N_1 transition suffers an increase. For higher temperatures, the PL integrated intensity of N_1 transition progressively decreases and the thermal extinction is observed at 170 K. This unexpected behaviour is illustrated in Fig. 3(a), and suggest a feeding mechanism in which, charge carriers are transferred from the radiative states involved in N_2 transition to the ones involved in N_1 transition.

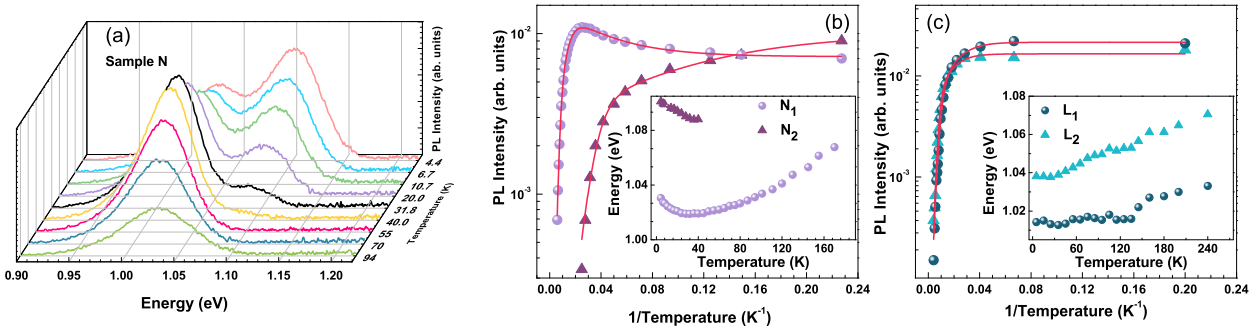

Figure 3: (a) PL spectra at different temperatures of N sample and dependence of the PL integrated intensity [(b), (c)] as well as of the peak energy [inserts in (b) and (c)] of (b) N and (c) L samples, on temperature. The lines in (b) and (c) illustrates the fits of Eq. 3 to the experimental data.

The dependence of the PL integrated intensity of each transition on temperature may be described considering the thermal activation of non-radiative de-excitation channels as the temperature is increased. This activation process is discussed in detail by Leitão *et al*,[50,51] and is described by the following equation:

$$I(T) = I_0 \left\{ \left[1 + \sum_i c_i \exp\left(-\frac{E_i}{kT}\right) + c_{\mathrm{bx}} T^{\frac{3}{2}} \exp\left(-\frac{E_{\mathrm{bx}}}{kT}\right) \right] \left[1 + \frac{g}{1 + c_{\mathrm{nr}} T^{\frac{3}{2}} \exp\left(-\frac{E_{\mathrm{nr}}}{kT}\right)} \right] \right\}^{-1}, \tag{3}$$

where k is the Boltzmann constant, and I_0 is a parameter related to the PL integrated intensity at 0 K [$I(0) = I_0/(1+g)$]. In the above equation, E_i and E_{bx} are the energy differences between the radiative state and a higher energy discrete level or an energy band, respectively. The term within the second pair of square brackets accounts for the possible thermal feeding of charge carriers by shallow traps, which are separated by an energy E_{nr} from the energy band.

Following Eq. 3, the analysis of the thermal quenching of the PL integrated intensity, for each radiative transition in the two samples, consider different models. The best fit for all investigated transitions, except N_1, was obtained considering two de-excitation channels: one involving a discrete excited state [i=1 in Eq. (3)] and another involving an energy band. For N_1 transition, evidence for only one de-excitation channel involving an energy band was found. In the latter case, an additional feeding mechanism was also considered in order to describe the increase of the PL integrated intensity in the low temperature regime [see spheres symbols in Fig. 3(b)]. The fits describe quite well the experimental trends in all sets of data [Fig. 3(b) and (c)] and the fitted parameters are presented in Table 2.

The insets in Fig. 3(b) and (c) depict the dependencies of the peak energy of the radiative transitions for both samples on temperature. For the N_1 transition, we observe a redshift for $T < 30$ K, followed by a blueshifht at a rate of 3.5×10^{-4} meV K^{-1}. For the N_2 transition, only a redshift is observed until its thermal extinction. For both transitions of L sample, just a blueshift is observed (on average, at a rate of 1.5×10^{-4} meV K^{-1}). We note again that the excitation power used with L sample is approximately six times greater than the one with N sample. For higher excitation powers, the thermal energy will contribute to populate states described by a higher value of the density of states (at higher energies). Consequently, the rate of the blueshift is lower than the one measured if the experiment is performed with a lower excitation power, which explains the reduction of the shift rate in L sample. Additionally, in the case of L sample, the absence of a redshift in the lower temperatures range is compatible with previous reports[41,44,52] showing that, with

the increase of the excitation power value, both the magnitude of the initial redshift and the temperature at which the change from red to blueshift occurs, decrease. Therefore, with respect to the dependence of the peak energy on temperature, we assume that both samples have qualitatively similar behaviours. Finally, we note that for N sample, the change from red to blueshift occurs for temperatures (30–40 K) lower than those usually reported (approximately 100 K).[18,28,41,49,53,54]

Table 2: Activation energies obtained from the fit of Eq. 3 to the data related to the dependence of the PL integrated intensity on temperature.

Sample	Transition	E_1 (meV)	E_{bx} (meV)	E_{nr} (meV)
N	N_1	–	18 ± 1	0.8 ± 0.5
	N_2	1.2 ± 0.2	10 ± 2	–
L	L_1	8 ± 1	37 ± 4	–
	L_2	10 ± 2	41 ± 13	–

Discussion

The shape of the luminescence of both samples, the obtained values for the β and m parameters, in addition to the redshift followed by a blueshift of the peak energy with the increment of the temperature (Fig. 3), are compatible with the presence of fluctuating potentials on both samples. However, there are several differences in the luminescence properties. From a structural and electronic points of view, the Ga-profile is the main difference between the two samples, and since both have a space charge region depth of ∼300 nm, the observed differences in the luminescence should be related mainly with the characteristics of the Ga-profiles, as will be discussed in the following sections.

Notch Ga-profile

In N sample, the two E_{bx} values (18 ± 1 and 10 ± 2 meV for N_1 and N_2 transitions, respectively) suggest a similar de-excitation channel involved in the thermal quenching of both

radiative transitions. These low energies are close to the experimental values ascribed in the literature to ionization energies of intrinsic shallow donors in CIGS.[55] However, due to the low effective mass of the electrons, it is not expected that single donors create bound states for electrons.[18,49] Thus, the de-excitation channels should involve the release of electrons from donors clusters, which create tails in the conduction band. The complete quenching of N_2 transition at approximately 40 K is compatible with the observed dependence of the peak energy with the increase of the excitation power for which two different slopes were observed: strong blueshift up to 10 mW, followed by an almost absence of shift for higher excitation powers. Considering the state filling effect,[42] the first slope should be related with the filling of a small density of states, whereas the absence of shift should be related with the complete filling of the involved states on that particular radiative transition. At this point, we must note that the energy shift of the luminescence is mainly dependent on the lower density of states describing the states occupied by electrons or holes. Additionally, it is also worth to mention that, in the case of holes, the density of states for an acceptor level or for tails in the valence band are always expected to be higher than the density of states for electrons.[56] Thus, if we assume the possible involvement of tails in the conduction band in the N_2 transition, we must ascribe the observed blueshift up to 10 mW to the low density of states describing the tails in the conduction band. The thermal extinction at a very low temperature is compatible with such a low density of states. Regarding N_1 transition, only one slope is observed in the dependence on the excitation power, which suggests a high enough density of states being filled. Therefore, in comparison with the case of N_2 transition, a higher density of states should be involved in N_1 transition.

The differences on the available density of states for the two transitions in N sample, can be explained assuming that they occur in regions with different depths in the sample. Hence, we must take into account the diffusion and drift of the free charge carriers throughout the sample promoted by the quasi-electric field related with the Ga-profile. There are two regions where it is more likely to occur recombinations in N sample,[10,26–28,57] i) near the CIGS/CdS

interface, and ii) at the notch where the conduction band minimum has its lowest value. The formation energy of defects depends on a balance between the composition and the Fermi energy level.[58] Since CIGS is a p-type material, the Fermi level is close to the top of the valence band. As the notch approaches, the Fermi level and the conduction band become progressively closer to each other, being the smallest separation in the notch. However, due to the inevitable appearance of donor defects on the surface of CIGS, in this region a small bending of the bands occurs that contributes in addition to the approximation between the Fermi level and the conduction band. Thus, the balance between the position of the Fermi level in these two regions (notch and CIGS/CdS interface), the different compositions, and the posterior deposition of the CdS layer, with the inevitable interdiffusion of atomic species between the CIGS and the CdS,[57] may favor the formation of the same type of defects, but with necessarily different densities in each region. Hereupon, the dependencies on the excitation power of N_1 and N_2 transitions may be explained in the following way. Assuming that at great extent the conduction band follows the Ga-profile,[14,15] electrons will occupy preferentially the region with lower GGI, where they recombine with holes (N_1 transition). At low temperatures, however, the reduced thermal energy will allow a small fraction of electrons to recombine near the CIGS/CdS interface (N_2 transition) where the density of states available for electrons is low, as discussed above. This interpretation is fully compatible with a drift of electrons in the conduction band, promoted by the increase of temperature, from near the CIGS/CdS interface to the notch. This region is more favorable from an energy point of view, thus contributing to N_1 transition. Such model is in accordance with the literature, in particular with reported time-resolved PL measurements at room temperature that identified a short lifetime (< 1 ns) component related with the CIGS/CdS interface, and a much longer lifetime component ascribed to the space charge region in the absorber layer.[26–28]

To further clarify the nature of the radiative recombination channels in N sample, and following the approach presented by Alonso *et al.*,[15] a qualitative calculation of the bandgap

energy value may be performed using the GGI values of 0.295 and 0.390, estimated from the Ga-profile, in the above discussed two regions of N sample. Accordingly, resulting bandgap energy values are $E_g(0.295) = 1.160\,\text{eV}$ for the notch region, and $E_g(0.390) = 1.214\,\text{eV}$ for the CIGS/CdS interface. Despite not being absolute values, their difference has a physical meaning. We should note that the difference between these two values (54 meV) is close to the difference between the peak energy of the two transitions at low temperature (72 meV) see Table 1. Thus, this result suggest that the two transitions have the same physical nature and occur in different regions of the CIGS layer: N_1 in the notch and N_2 near the CIGS/CdS interface.

The spectroscopic energy difference between bandgap and peak energies in each of the two regions are $E_g(0.295)$-$E_p^{N_1} = 0.142\,\text{eV}$ and $E_g(0.390)$-$E_p^{N_2} = 0.124\,\text{eV}$. The combination of those high energy separations with the energies estimated for the shallow tails states in the conduction band (18 and 10 meV for N_1 and N_2 transitions, respectively) suggests that both transitions involve a hole located at a deep enough acceptor level. Hence, the N_1 and N_2 radiative transitions that occur in the notch and near the CIGS/CdS interface, respectively, are both ascribed to a tail-impurity (TI) transition involving the same acceptor level and similar donors clusters, i.e., a recombination of electrons trapped in tails in the conduction band with holes bound to a deep acceptor level that follows the fluctuating potentials of the valence band, as schematically illustrated in Fig. 4(a). Note that Fig. 4 intends to be a phenomenological representation of the radiative transitions in both samples. Therefore, in order to have a sufficiently clear illustration of the impact of the Ga-profiles on the in-depth electronic energy levels structure, the fluctuating potentials were assumed as periodic which, obviously, is not the actual profile of the fluctuations in the real space. For the same reason, the energetic position of the acceptor impurity band is not scaled at its ionization energy.

In order to further discuss the possible transfer of charge carriers between the radiative states involved in the N_2 transition to the radiative states involved in the N_1 transition (see Fig. 3(a)), we follow a common analysis for lightly doped semiconductors when for a particu-

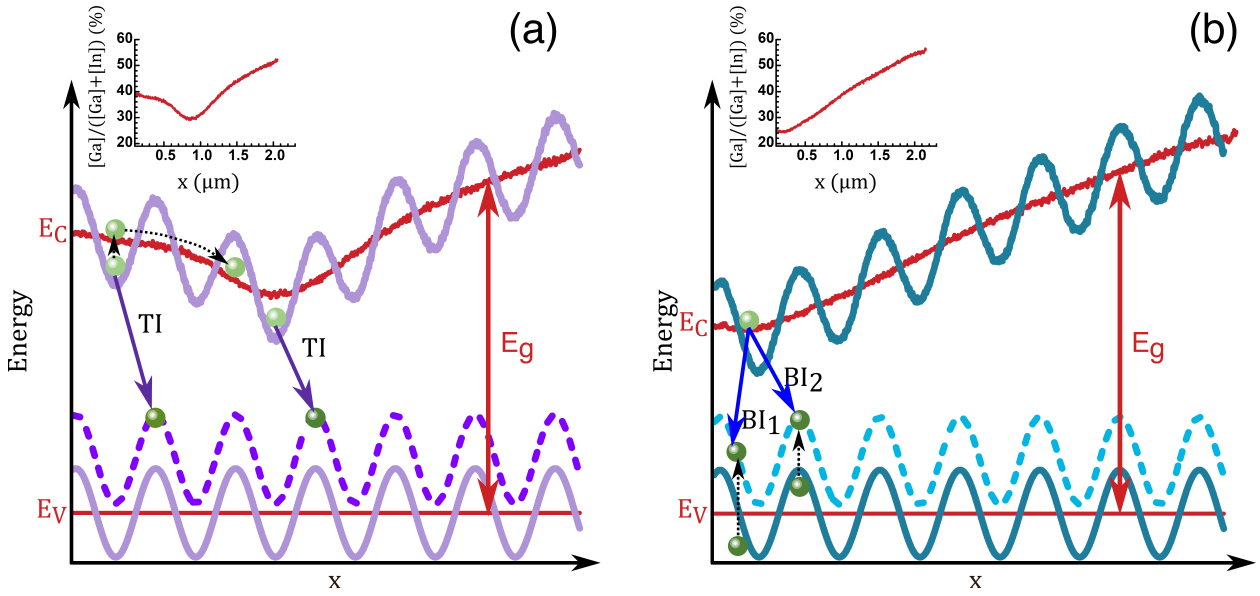

Figure 4: Schematic illustration of the proposed models for the electronic energy level structures for (a) N and (b) L samples. E_C, E_V, and E_g represent the percolation level for electrons and holes, and the bandgap energy of the doped semiconductor, respectively. The dashed lines stands for an acceptor impurity level that is not energetically scaled. In (a), the TI transition represents radiative transitions involving a shallow donor cluster and a sufficient deep acceptor impurity level. In (b), BI_1 and BI_2 represent two types of radiative recombination involving the same acceptor level of a hole located in regions of the material where the top of the valence band is located below and above the percolation level, respectively. These energy schemes are in-depth phenomenological illustrations to emphasize the impact of the Ga-profile on the electronic energy level structures.

lar optical center, two excited and radiative states can be found in thermal equilibrium.[59–61] In such a case, the ratio between the PL integrated intensity from those two hypothetical radiative states can be expressed by a Boltzmann factor. In the case of our sample, the existence of the notch Ga-profile prevents the establishment of a true thermal equilibrium between the radiative states involved in the two transitions, but the theoretical model can be adapted according to the physical characteristics of the Ga-profile. Taking into account the TI transitions assumed previously (see Fig. 4(a)), the increase of temperature will result in the release of electrons from the tails near the CIGS/CdS interface to the conduction band in that region. The shape of the Ga-profile causes the released electrons to move to the notch region where they can be captured in the tails, thus giving rise to the N_2 transition. The electrons that were already in the notch region can be released to the conduction band

but the shape of the Ga-profile blocks its diffusion to other regions of the sample. As a consequence, the intensities ratio of the two transitions is dependent on the temperature and can be described by a Boltzmann factor. In Fig. 5, we plot the dependence on temperature of the logarithm of the ratio of PL integrated intensities of N_1 and N_2 transitions ($I_{N_1}(T)/I_{N_2}(T)$). As can be seen, in the temperature range 20-40 K, where the change of the PL integrated intensity of both transitions is more notorious, a linear behaviour is observed. The experimental points were fitted with a Boltzmann factor

$$\frac{I_{N_1}(T)}{I_{N_2}(T)} = \frac{I_{N_1}(\infty)}{I_{N_2}(\infty)} \exp\left(-\frac{\Delta E}{kT}\right), \tag{4}$$

where $I_{N_1}(\infty)/I_{N_2}(\infty)$ ratio for the limit of $T \to \infty$ is proportional to the ratio between the probabilities of recombination from the radiative states in the two regions of the sample. In the case of a TI transition, ΔE reflects the energy difference between the tail state and the conduction band, as schematically illustrated in the inset of Fig. 5. From the fit of Eq. 4 to the experimental data in the high temperature regime, we obtained $\Delta E = 13 \pm 2$ meV which is within the error estimated for E_{bx} for the N_2 transition. Regarding the ratio $I_{N_1}(\infty)/I_{N_2}(\infty)$, a value of 647±65 was found, which is in accordance with a much higher probability of radiative recombination in the notch region in comparison with near the CIGS/CdS interface region of the Ga-profile. Thus, these results further supports the TI-type radiative transition assumed for the notch Ga-profile.

Linear Ga-profile

L sample have a Ga-profile characterized by an in-depth continuous increase of Ga, which promotes the diffusion of electrons to the superficial layer of the CIGS, near to the CIGS/CdS interface. As a consequence, the observed radiative transitions should come from a region of approximately 300 nm near that surface and associated to an almost constant bandgap energy. The two E_{bx} activation energies are close to each other, 37 ± 4 meV and $41 \pm$

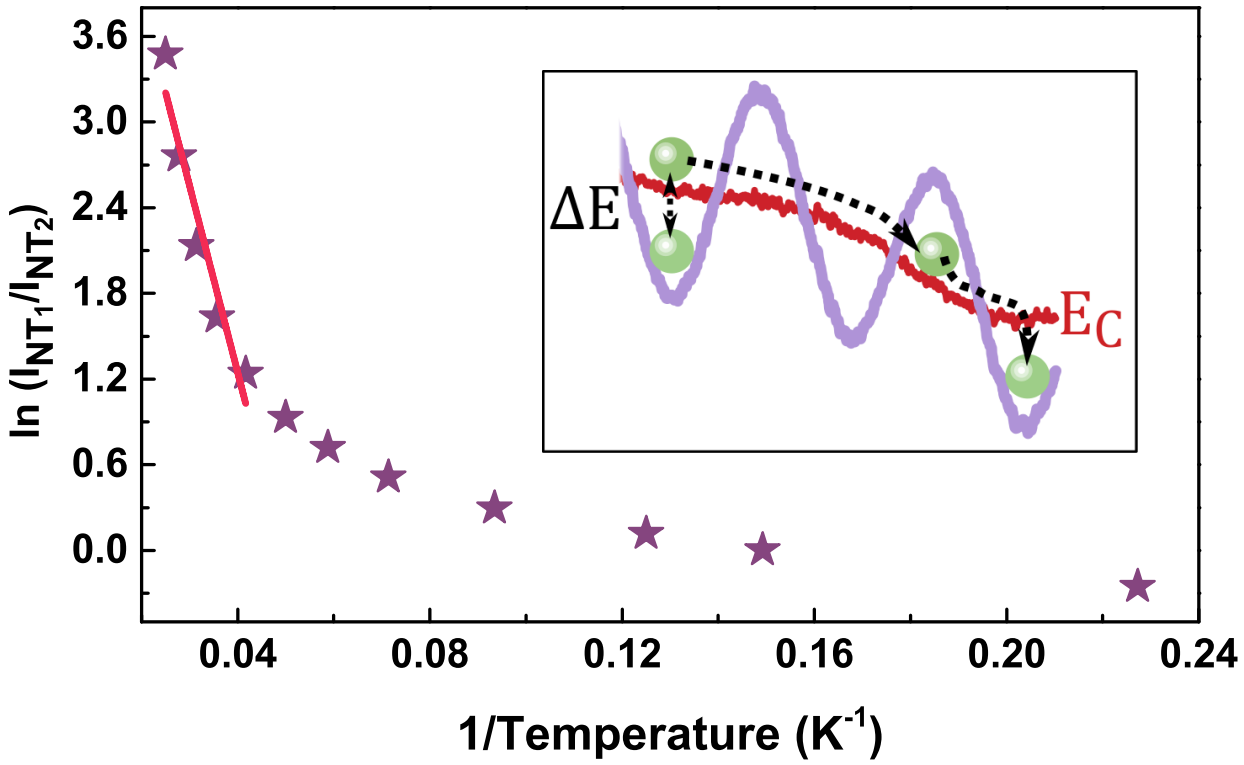

Figure 5: Dependence on temperature of the PL integrated intensity of $\ln(I_{N_1}/I_{N_2})$. The inset illustrates a scheme of the thermally-induced feeding mechanism. Here, E_C stands for the percolation level for the electrons; and ΔE reflects the energy difference between the tail state and the conduction band.

13 meV, which suggest the thermal activation of the same de-excitation channel. These E_{bx} values are also close to the ionization energy values obtained experimentally for CIGS samples with linear Ga-profile[18] and calculated theoretically for the V_{Cu} acceptor defect (30 meV).[58,62] Taking into account these facts, and given the almost constant bandgap energy in the superficial region, the observation of the two radiative transitions involving the same defect cannot be explained by assuming different bandgap energy values for each transition, as done for the N sample. In fact, we propose that both transitions for L sample may be ascribed to a band-impurity (BI) transition,[47,56] in which the hole must be bound to an acceptor state. For high enough temperatures, holes may be released to the valence band, which is reflected in the quenching of the luminescence. The E_{bx} activation energy parameterizes this process. Nevertheless, in highly doped materials, we may distinguish two types of BI transitions involving the same acceptor level,[56] which depend on the location of the top of valence band relatively to the percolation level. Depending on the region of the material, we may have the top of the valence band located below or above the percolation level [see Fig. 4(b)] corresponding to BI_1 and BI_2 transitions, respectively.[56] At low temperatures and under a low excitation power, the hole should be located in the lower available states, so only the BI_2 transition is expected. However, the observation of the BI_1 transition in our measurements at low temperature, is due to the high enough excitation power to fill the acceptor levels up to energies in which the valence band is below the percolation level. Thus, transitions L_1 and L_2 may be ascribed to a BI_2 and BI_1 transitions, respectively, as schematically illustrated in Fig. 4(b).

The dependence on temperature of the peak energy of both transitions corroborates the above model. Increasing the temperature, the two transitions start showing no shift and after a particular temperature ($\sim$ 135 K and $\sim$ 25 K for L_1 and L_2 transitions, respectively), a blueshift is observed. The difference in the temperature of the beginning of the blueshift may be understood if we take into account the occupation level of the acceptor levels by holes. In the case of L_2 transition (BI_1), the involved holes have a higher energies (from

the point of view of this charge carrier) than the ones involved in L_1 transition. Thus, with the increase of the temperature in a low values regime ($T \lesssim 135$ K), the unoccupied energy states available for holes can only the reached by the holes involved in L_2 transition because the thermal energy is not enough to release holes from deeper states to the empty ones. This justifies the blueshift of L_1 transition only for $T \gtrsim 135$ K and not for a much lower temperature as observed for the L_2 transition. To this behaviour contributes the fact that, as discussed above, the excitation power used in the temperature dependence of the luminescence of L sample was significantly higher than for N sample.

Regarding the influence of the fluctuating potentials, L sample presents lower β values and the shape of the luminescence is slightly less asymmetric comparing with N sample, which suggests a lower influence of fluctuating potentials. As shown in Fig. 4, the characteristics of the Ga-profile influence the inspected region by PL, which means different densities of defects were accessed in the two samples. However, this experimental evidence is not reflected in the electrical parameters, since the obtained V_{OC} losses are approximately the same for the two samples, 451 and 449 mV for N and L samples, respectively.[11] Thus, the comparison of the influence of fluctuating potentials between the studied samples is not straightforward.

Our results show a significant influence of the Ga-profile on the radiative and non-radiative recombination channels as well as on the dynamics of the charge carriers. For a notch Ga-profile, the drift of electrons to the notch region is favored, which is reflected in a significantly higher probability of recombination in this region. For the linear Ga-profile, the recombination at a superficial region near the CIGS/CdS interface is more likely to happen, since the drift of the electrons into the CIGS bulk region is not favored by this Ga-profile. Regarding the radiative recombination channels for the two Ga-profiles, we showed that the physical nature of the transitions is quite different in the two samples, despite the similar spectroscopic energy of the dominant transitions. In the case of N sample, a deep acceptor is involved whereas for the L sample the dominant acceptor level is significantly shallower. The aforementioned in-depth experimental identification of the effect of the elemental profiling

is of the utmost importance as it provides evidence for the need of further optimization of such feature in state-of-the-art devices.

Conclusions

In summary, a deep investigation of CIGS thin films with two different Ga-profiles (notch and linear) by PL was performed in order identify dominant radiative and non-radiative recombination channels and discuss the charge carriers dynamics for both Ga-profiles. Two CIGS based samples, one with a notch Ga-profile (N sample) and another with a linear Ga-profile (L sample), were studied. The dependence on the excitation power and temperature of the PL for both Ga-profiles revealed significant differences in the dominant radiative and non-radiative recombination channels in each case. In both samples, two radiative transitions involving fluctuating potentials were identified. For the sample with a notch Ga-profile, the radiative transitions occur in the notch and near the CIGS surface. Both were ascribed to a TI type transition involving the same deep acceptor level and similar donors clusters. For the sample with a linear Ga-profile, the radiative transitions were ascribed to a BI_2 and BI_1 transitions, compatible with the involvement of the V_{Cu} defect. Steady state PL measurements gave a quantitative evidence for the difference in probability of recombination from the superficial and notch regions in the notch Ga-profile whereas, for the linear Ga-profile, only radiative recombination related with a superficial region near the CIGS/CdS interface was detected. This work also shows the importance of a careful control of the experimental parameters in a steady-state PL experiment in order to allow a deep enough exploitation of the electronic structure.

Acknowledgements

This work was developed within the scope of the project i3N, UIDB/50025/2020 & UIDP/50025/2020, and POCI-01-0145-FEDER-007688 financed by national funds through the “Fundação para

a Ciência e a Tecnologia" (FCT)/MEC, by FEDER funds through the COMPETE 2020 Programme, and the ERDF through COMPETE2020 under the project NovaCell – Development of novel Ultrathin Solar Cell Architectures for low-light, low-cost, and flexible opto-electronic devices (action number 28075), InovSolarCells – Development of innovative nanostructured dielectric materials for interface passivation in thin film solar cells project (action number 29696), "Programa Operacional Regional do Centro (Centro2020)" through FEDER in the partnership PT2020 under the project SusPhotoSolutions - "Soluções Fotovoltaicas Sustentáveis", and the European Union's Horizon 2020 research and innovation programme ARCIGS-M project (grant agreement no. 720887). P. M. P. Salomé thanks the funding of FCT through the project IF/00133/2015.

References

(1) Solar Frontier, Press Release, Japan, January 17, 2019.

(2) Jackson, P.; Wuerz, R.; Hariskos, D.; Lotter, E.; Witte, W.; Powalla, M. Effects of heavy alkali elements in Cu(In,Ga)Se2 solar cells with efficiencies up to 22.6%. *physica status solidi (RRL) – Rapid Research Letters* **2016**, *10*, 583–586.

(3) Jackson, P.; Hariskos, D.; Wuerz, R.; Kiowski, O.; Bauer, A.; Friedlmeier, T. M.; Powalla, M. Properties of Cu(In,Ga)Se2 solar cells with new record efficiencies up to 21.7%. *physica status solidi (RRL) – Rapid Research Letters* **2015**, *9*, 28–31.

(4) Kato, T.; Wu, J.; Hirai, Y.; Sugimoto, H.; Bermudez, V. Record Efficiency for Thin-Film Polycrystalline Solar Cells Up to 22.9% Achieved by Cs-Treated Cu(In,Ga)(Se,S)2. *IEEE Journal of Photovoltaics* **2019**, *9*, 325–330.

(5) Nishiwaki, M.; Nagaya, K.; Kato, M.; Fujimoto, S.; Tampo, H.; Miyadera, T.; Chikamatsu, M.; Shibata, H.; Fujiwara, H. Tail state formation in solar cell materials: First

principles analyses of zincblende, chalcopyrite, kesterite, and hybrid perovskite crystals. *Phys. Rev. Materials* **2018**, *2*, 085404.

(6) Teixeira, J. P.; Salomé, P. M. P.; Alves, B.; Edoff, M.; Leitão, J. P. Evidence of Limiting Effects of Fluctuating Potentials on V_{OC} of Cu(In, Ga)Se_2 Thin-Film Solar Cells. *Phys. Rev. Applied* **2019**, *11*, 054013.

(7) Lundberg, O.; Edoff, M.; Stolt, L. The effect of Ga-grading in CIGS thin film solar cells. *Thin Solid Films* **2005**, *480-481*, 520 – 525.

(8) Kaufmann, C.; Caballero, R.; Unold, T.; Hesse, R.; Klenk, R.; Schorr, S.; Nichterwitz, M.; Schock, H.-W. Depth profiling of Cu(In,Ga)Se_2 thin films grown at low temperatures. *Solar Energy Materials and Solar Cells* **2009**, *93*, 859 – 863.

(9) Schleussner, S. M.; Törndahl, T.; Linnarsson, M.; Zimmermann, U.; Wätjen, T.; Edoff, M. Development of gallium gradients in three-stage Cu(In,Ga)Se_2 co-evaporation processes. *Progress in Photovoltaics: Research and Applications* **2012**, *20*, 284–293.

(10) Chirilă, A.; Buecheler, S.; Pianezzi, F.; Bloesch, P.; Gretener, C.; Uhl, A. R.; Fella, C.; Kranz, L.; Perrenoud, J.; Seyrling, S. et al. Highly efficient Cu(In,Ga)Se_2 solar cells grown on flexible polymer films. *Nat. Mater.* **2011**, *10*, 857.

(11) Salomé, P. M.; Fjällström, V.; Szaniawski, P.; Leitão, J. P.; Hultqvist, A.; Fernandes, P. A.; Teixeira, J. P.; Falcão, B. P.; Zimmermann, U.; da Cunha, A. F. et al. A comparison between thin film solar cells made from co-evaporated $CuIn_{1-x}Ga_xSe_2$ using a one-stage process versus a three-stage process. *Progress in Photovoltaics: Research and Applications* **2015**, *23*, 470–478.

(12) Feurer, T.; Reinhard, P.; Avancini, E.; Bissig, B.; Löckinger, J.; Fuchs, P.; Carron, R.; Weiss, T. P.; Perrenoud, J.; Stutterheim, S. et al. Progress in thin film CIGS photovoltaics – Research and development, manufacturing, and applications. *Progress in Photovoltaics: Research and Applications* **2017**, *25*, 645.

(13) Alberto, H. V.; Vilão, R. C.; Vieira, R. B. L.; Gil, J. M.; Weidinger, A.; Sousa, M. G.; Teixeira, J. P.; da Cunha, A. F.; Leitão, J. P.; Salomé, P. M. P. et al. Slow-muon study of quaternary solar-cell materials: Single layers and $p-n$ junctions. *Phys. Rev. Materials* **2018**, *2*, 025402.

(14) Wei, S.-H.; Zunger, A. Band offsets and optical bowings of chalcopyrites and Zn-based II-IV alloys. *J. Appl. Phys.* **1995**, *78*, 3846–3856.

(15) Alonso, M. I.; Garriga, M.; Durante Rincón, C. A.; Hernández, E.; León, M. Optical functions of chalcopyrite $CuGa_xIn_{1-x}Se_2$ alloys. *Applied Physics A* **2002**, *74*, 659–664.

(16) Dullweber, T.; Lundberg, O.; Malmström, J.; Bodegård, M.; Stolt, L.; Rau, U.; Schock, H.; Werner, J. Back surface band gap gradings in Cu(In,Ga)Se_2 solar cells. *Thin Solid Films* **2001**, *387*, 11–13.

(17) Salomé, P.; Keller, J.; Törndahl, T.; Teixeira, J.; Nicoara, N.; Andrade, R.-R.; Stroppa, D.; González, J.; Edoff, M.; Leitão, J. et al. CdS and $Zn_{1-x}Sn_xO_y$ buffer layers for CIGS solar cells. *Solar Energy Materials and Solar Cells* **2017**, *159*, 272 – 281.

(18) Salomé, P. M. P.; Teixeira, J. P.; Keller, J.; Törndahl, T.; Sadewasser, S.; Leitão, J. P. Influence of CdS and ZnSnO Buffer Layers on the Photoluminescence of Cu(In,Ga)Se_2 Thin Films. *IEEE Journal of Photovoltaics* **2017**, *7*, 670–675.

(19) Topič, M.; Smole, F.; Furlan, J. Band-gap engineering in CdS/Cu(In,Ga)Se_2 solar cells. *Journal of Applied Physics* **1996**, *79*, 8537–8540.

(20) Song, J.; Li, S. S.; Huang, C.; Crisalle, O.; Anderson, T. Device modeling and simulation of the performance of Cu(In: $1-x$,Ga_x)Se_2 solar cells. *Solid-State Electronics* **2004**, *48*, 73 – 79.

(21) Gloeckler, M.; Sites, J. Band-gap grading in Cu(In,Ga)Se_2 solar cells. *Journal of Physics and Chemistry of Solids* **2005**, *66*, 1891 – 1894.

(22) Frisk, C.; Platzer-Björkman, C.; Olsson, J.; Szaniawski, P.; Wätjen, J. T.; Fjällström, V.; Salomé, P.; Edoff, M. Optimizing Ga-profiles for highly efficient Cu(In,Ga)Se_2 thin film solar cells in simple and complex defect models. *Journal of Physics D: Applied Physics* **2014**, *47*, 485104.

(23) Hirai, Y.; Kurokawa, Y.; Yamada, A. Numerical study of Cu(In,Ga)Se_2 solar cell performance toward 23% conversion efficiency. *Japanese Journal of Applied Physics* **2013**, *53*, 012301.

(24) Aissat, A.; Arbouz, H.; Vilcot, J. Optimization and improvement of a front graded bandgap $CuInGaSe_2$ solar cell. *Solar Energy Materials and Solar Cells* **2018**, *180*, 381 – 385.

(25) Pawłowski, M.; Zabierowski, P.; Bacewicz, R.; Barreau, N. Influence of Ga-notch position on recombination processes in Cu(In,Ga)Se_2-based solar cells investigated by means of photoluminescence. *Thin Solid Films* **2013**, *535*, 336 – 339.

(26) Kuciauskas, D.; Li, J. V.; Contreras, M. A.; Pankow, J.; Dippo, P.; Young, M.; Mansfield, L. M.; Noufi, R.; Levi, D. Charge carrier dynamics and recombination in graded band gap $CuIn_{1-x}Ga_xSe_2$ polycrystalline thin-film photovoltaic solar cell absorbers. *Journal of Applied Physics* **2013**, *114*, 154505.

(27) Kuciauskas, D.; Li, J. V.; Kanevce, A.; Guthrey, H.; Contreras, M.; Pankow, J.; Dippo, P.; Ramanathan, K. Charge-carrier dynamics in polycrystalline thin-film $CuIn_{1-x}Ga_xSe_2$ photovoltaic devices after pulsed laser excitation: Interface and space-charge region analysis. *Journal of Applied Physics* **2015**, *117*, 185102.

(28) Jensen, S. A.; Glynn, S.; Kanevce, A.; Dippo, P.; Li, J. V.; Levi, D. H.; Kuciauskas, D.

Beneficial effect of post-deposition treatment in high-efficiency Cu(In,Ga)Se_2 solar cells through reduced potential fluctuations. *Journal of Applied Physics* **2016**, *120*, 063106.

(29) Novikov, G. F.; Gapanovich, M. V. Third-generation Cu-In-Ga-(S, Se)-based solar inverters. *Physics-Uspekhi* **2017**, *60*, 161–178.

(30) Ando, Y.; Ishizuka, S.; Wang, S.; Chen, J.; Islam, M. M.; Shibata, H.; Akimoto, K.; Sakurai, T. Relationship between bandgap grading and carrier recombination for Cu(In,Ga)Se_2-based solar cells. *Japanese Journal of Applied Physics* **2018**, *57*, 08RC08.

(31) Nam, Y.; Yoo, J.; Chang, S. K.; Wi, J.-H.; Lee, W.-J.; Cho, D.-H.; Chung, Y.-D. Photoluminescence of sulfur-incorporated CIGS solar cells through post-annealing. *Journal of Luminescence* **2017**, *188*, 595 – 599.

(32) Parravicini, J.; Acciarri, M.; Murabito, M.; Donne, A. L.; Gasparotto, A.; Binetti, S. In-depth photoluminescence spectra of pure CIGS thin films. *Appl. Opt.* **2018**, *57*, 1849–1856.

(33) Shirakata, S.; Ohkubo, K.; Ishii, Y.; Nakada, T. Effects of CdS buffer layers on photoluminescence properties of Cu(In,Ga)Se_2 solar cells. *Solar Energy Materials and Solar Cells* **2009**, *93*, 988 – 992.

(34) Shin, D.; Kim, J.; Gershon, T.; Mankad, R.; Hopstaken, M.; Guha, S.; Ahn, B. T.; Shin, B. Effects of the incorporation of alkali elements on Cu(In,Ga)Se_2 thin film solar cells. *Solar Energy Materials and Solar Cells* **2016**, *157*, 695 – 702.

(35) Wolter, M. H.; Bissig, B.; Avancini, E.; Carron, R.; Buecheler, S.; Jackson, P.; Siebentritt, S. Influence of Sodium and Rubidium Postdeposition Treatment on the Quasi-Fermi Level Splitting of Cu(In,Ga)Se_2 Thin Films. *IEEE Journal of Photovoltaics* **2018**, *8*, 1320–1325.

(36) Okano, M.; Takabayashi, Y.; Sakurai, T.; Akimoto, K.; Shibata, H.; Niki, S.; Kanemitsu, Y. Slow intraband relaxation and localization of photogenerated carriers in $CuIn_{1-x}Ga_xSe_2$ thin films: Evidence for the existence of long-lived high-energy carriers. *Phys. Rev. B* **2014**, *89*, 195203.

(37) Yu, P. W. Excitation-dependent emission in Mg-, Be-, Cd-, and Zn-implanted GaAs. *Journal of Applied Physics* **1977**, *48*, 5043–5051.

(38) Teixeira, J. P.; Sousa, R. A.; Sousa, M. G.; da Cunha, A. F.; Fernandes, P. A.; Salomé, P. M. P.; González, J. C.; Leitão, J. P. Comparison of fluctuating potentials and donor-acceptor pair transitions in a Cu-poor Cu_2ZnSnS_4 based solar cell. *Applied Physics Letters* **2014**, *105*, 163901.

(39) Teixeira, J. P.; Sousa, R. A.; Sousa, M. G.; da Cunha, A. F.; Fernandes, P. A.; Salomé, P. M. P.; González, J. C.; Leitão, J. P. Erratum: "Comparison of fluctuating potentials and donor-acceptor pair transitions in a Cu-poor Cu_2ZnSnS_4 based solar cell" [Appl. Phys. Lett. 105, 163901 (2014)]. *Applied Physics Letters* **2015**, *107*, 049903.

(40) Ben Sedrine, N.; Ribeiro-Andrade, R.; Gustafsson, A.; Soares, M. R.; Bourgard, J.; Teixeira, J. P.; Salomé, P. M. P.; Correia, M. R.; Moreira, M. V. B.; De Oliveira, A. G. et al. Fluctuating potentials in GaAs:Si nanowires: critical reduction of the influence of polytypism on the electronic structure. *Nanoscale* **2018**, *10*, 3697–3708.

(41) Schumacher, S. A.; Botha, J. R.; Alberts, V. Photoluminescence study of potential fluctuations in thin layers of $Cu(In_{0.75}Ga_{0.25})(S_ySe_{1-y})_2$. *Journal of Applied Physics* **2006**, *99*, 063508.

(42) Lang, M.; Zimmermann, C.; Krämmer, C.; Renz, T.; Huber, C.; Kalt, H.; Hetterich, M. Luminescence properties of $Cu_2ZnSn(S,Se)_4$ solar cell absorbers: State filling versus screening of electrostatic potential fluctuations. *Phys. Rev. B* **2017**, *95*, 155202.

(43) Lang, M.; Renz, T.; Opolka, A.; Zimmermann, C.; Krämmer, C.; Neuwirth, M.; Kalt, H.; Hetterich, M. Impact of the degree of Cu–Zn order in $Cu_2ZnSn(S,Se)_4$ solar cell absorbers on defect states and band tails. *Applied Physics Letters* **2018**, *113*, 033901.

(44) Levanyuk, A. P.; Osipov, V. V. Edge luminescence of direct-gap semiconductors. *Soviet Physics Uspekhi* **1981**, *24*, 187–215.

(45) Schmidt, T.; Lischka, K.; Zulehner, W. Excitation-power dependence of the near-band-edge photoluminescence of semiconductors. *Phys. Rev. B* **1992**, *45*, 8989–8994.

(46) Teixeira, J. P.; Salomé, P. M. P.; Sousa, M. G.; Fernandes, P. A.; Sadewasser, S.; da Cunha, A. F.; Leitão, J. P. Optical and structural investigation of Cu_2ZnSnS_4 based solar cells. *physica status solidi (b)* **2016**, *253*, 2129–2135.

(47) Leitão, J. P.; Santos, N. M.; Fernandes, P. A.; Salomé, P. M. P.; da Cunha, A. F.; González, J. C.; Ribeiro, G. M.; Matinaga, F. M. Photoluminescence and electrical study of fluctuating potentials in Cu_2ZnSnS_4-based thin films. *Phys. Rev. B* **2011**, *84*, 024120.

(48) Bleuse, J.; Ducroquet, F.; Mariette, H. Potential Fluctuations and Localization Effects in CZTS Single Crystals, as Revealed by Optical Spectroscopy. *Journal of Electronic Materials* **2018**, *47*, 4282–4288.

(49) Teixeira, J. P.; Sousa, R. A.; Sousa, M. G.; da Cunha, A. F.; Fernandes, P. A.; Salomé, P. M. P.; Leitão, J. P. Radiative transitions in highly doped and compensated chalcopyrites and kesterites: The case of Cu_2ZnSnS_4. *Phys. Rev. B* **2014**, *90*, 235202.

(50) Leitão, J. P.; Carmo, M. C.; Henry, M. O.; McGlynn, E. Uniaxial stress study of the $1026 - \mathrm{meV}$ center in $Si : Pt$. *Phys. Rev. B* **2001**, *63*, 235208.

(51) Leitão, J. P.; Carvalho, A.; Coutinho, J.; Pereira, R. N.; Santos, N. M.; Ankiewicz, A. O.; Sobolev, N. A.; Barroso, M.; Lundsgaard Hansen, J.; Nylandsted Larsen, A. et al. Influence of Ge content on the optical properties of X and W centers in dilute Si-Ge alloys. *Phys. Rev. B* **2011**, *84*, 165211.

(52) Larsen, J. K.; Burger, K.; Gütay, L.; Siebentritt, S. Temperature dependence of potential fluctuations in chalcopyrites. 2011 37th IEEE Photovoltaic Specialists Conference. 2011; pp 000396–000401.

(53) Park, S. H.; Choe, B. D. Interimpurity transitions in heavily doped semiconductors. *Journal of Applied Physics* **1990**, *68*, 5916–5918.

(54) Dirnstorfer, I.; Wagner, M.; Hofmann, D. M.; Lampert, M. D.; Karg, F.; Meyer, B. K. Characterization of CuIn(Ga)Se_2 Thin Films. *physica status solidi (a)* **1998**, *168*, 163–175.

(55) Siebentritt, S.; Rega, N.; Zajogin, A.; Lux-Steiner, M. C. Do we really need another PL study of $CuInSe_2$? *physica status solidi (c)* **2004**, *1*, 2304–2310.

(56) Osipov, V. V.; Soboleva, T. I.; Foigel, M. G. Interimpurity radiative recombination in heavily doped semiconductors. *Sov. Phys. Semicond.* **1977**, *11*, 752.

(57) Salomé, P. M. P.; Ribeiro-Andrade, R.; Teixeira, J. P.; Keller, J.; Törndahl, T.; Nicoara, N.; Edoff, M.; González, J. C.; Leitão, J. P.; Sadewasser, S. Cd and Cu Interdiffusion in Cu(In,Ga)Se_2/CdS Hetero-Interfaces. *IEEE Journal of Photovoltaics* **2017**, *7*, 858–863.

(58) Zhang, S. B.; Wei, S.-H.; Zunger, A.; Katayama-Yoshida, H. Defect physics of the $CuInSe_2$ chalcopyrite semiconductor. *Phys. Rev. B* **1998**, *57*, 9642–9656.

(59) Càlão, M. I.; do Carmo, M. C. Luminescence from an iron related deep centre in silicon. *Physica Scripta* **1988**, *38*, 455–457.

(60) Nazaré, M. H.; Carmo, M. C.; Duarte, A. J. Luminescence from transition metal centres in silicon doped with silver and nickel. *Materials Science and Engineering: B* **1989**, *4*, 273 – 276.

(61) Henry, M. O.; Campion, J. D.; McGuigan, K. G.; Lightowlers, E. C.; do Carmo, M. C.; Nazaré, M. H. A photoluminescence study of Zn-O complexes in silicon. *Semiconductor Science and Technology* **1994**, *9*, 1375–1381.

(62) Wei, S.-H.; Zhang, S. B.; Zunger, A. Effects of Ga addition to $CuInSe_2$ on its electronic, structural, and defect properties. *Applied Physics Letters* **1998**, *72*, 3199–3201.